

Direct Imaging of High-Frequency Multimode Spin Wave Propagation in Cobalt-Iron Waveguides Using X-Ray Microscopy beyond 10 GHz

Nick Träger,* Paweł Gruszecki, Filip Lisiecki, Johannes Förster, Markus Weigand, Sebastian Wintz, Hermann Stoll, Hubert Głowiński, Piotr Kuświk, Maciej Krawczyk, and Joachim Gräfe*

Not only in fundamental wave physics but also in technical areas such as radar and communication systems, high-frequency magnonics is increasingly attracting attention. Here, time-resolved scanning transmission X-ray microscopy is used to directly image high-frequency spin wave propagation in cobalt-iron waveguides at excitation frequencies above 10 GHz. In addition, an excitation technique is presented, which allows for versatile pump–probe experiments with radio frequency currents up to 30 GHz. With this approach, a global sinusoidal magnetic field excitation is applied to induce spin waves from the waveguide edges. Amplitude, relative phase, and k -space information as a function of excitation frequencies and static external fields are observed, matching the theoretical predictions for confined waveguide structures. In doing so, the foundation for high-frequency multimode spin wave excitation and propagation at the nanoscale is laid, which can be a prospective path in radar and communication systems.

The rising research field of magnonics, which is named after the quanta of spin waves, represents a potential candidate for substituting electronic devices as information carriers at the nanoscale.^[1–5] Nevertheless, data communication does not represent the only prospective route for magnonics. High-frequency radar systems get increasingly important, e.g., for autonomous driving. This requires very accurate and fast position tracking as well as communication with surrounding vehicles.^[6] However, complex electronic building blocks for radar

transceivers are vulnerable for nonlinearities at high frequencies and, thus, cause serious problems regarding reliable detection and communication.^[6–9] With respect to higher stability, higher data throughput, and faster logic operations at frequencies above 10 GHz, magnonic circuits represent a very promising approach, which allows for substituting several electronic elements in current radar systems.^[10]


Radar sensors typically require a larger signal bandwidth than communication signals. Thus, high performance in both radar and communication applications requires fine-tuning of signals and advanced bandwidth concepts. Therefore, single- and multi-carrier waveforms between 20 and 30 GHz are very promising for increasing transmission rates and combining commu-

nication and sensing.^[6] To this end, magnonic waveguides show outstanding characteristics for reliable multimode propagation,^[11–14] which could define the backbone of magnonic building blocks in prospective radar applications.^[3,15]

In this work, we demonstrate the spatially and temporally resolved observation of spin wave excitation and propagation in such magnonic cobalt-iron (CoFe) waveguides at the nanoscale by time-resolved scanning transmission X-ray microscopy (STXM). The large saturation magnetization of CoFe results

N. Träger, J. Förster, Dr. S. Wintz, Dr. H. Stoll, Dr. J. Gräfe
Modern Magnetic Systems
Max Planck Institute for Intelligent Systems
Heisenbergstraße 3, 70569 Stuttgart, Germany
E-mail: traeger@is.mpg.de; graefe@is.mpg.de

Dr. P. Gruszecki, Prof. M. Krawczyk
Faculty of Physics
Adam Mickiewicz University
ul. Uniwersytetu Poznańskiego 2, 61-614 Poznań, Poland

 The ORCID identification number(s) for the author(s) of this article can be found under <https://doi.org/10.1002/pssr.202000373>.

© 2020 The Authors. Published by Wiley-VCH GmbH. This is an open access article under the terms of the Creative Commons Attribution License, which permits use, distribution and reproduction in any medium, provided the original work is properly cited.

DOI: 10.1002/pssr.202000373

Dr. P. Gruszecki, Dr. F. Lisiecki, Dr. H. Głowiński, Dr. P. Kuświk
Institute of Molecular Physics
Polish Academy of Sciences
Mariana Smoluchowskiego 17, 60-179 Poznań, Poland

Dr. M. Weigand
Helmholtz-Zentrum Berlin
Albert-Einstein-Straße 15, 12489 Berlin, Germany

Dr. S. Wintz
Laboratory for Condensed Matter
Paul Scherrer Institute
Forschungsstrasse 111, 5232 Villigen PSI, Switzerland

Dr. H. Stoll
Institute of Physics
Johannes Gutenberg-Universität Mainz
Staudingerweg 7, 55128 Mainz, Germany

in a shift to higher resonance frequencies compared with other conventional materials, for example, permalloy (FeNi). For spin wave excitation, a global sinusoidal radio frequency (RF) current is generated by an arbitrary waveform generator. The resulting RF magnetic field leads to the emission of magnons from the waveguide edges.^[16,17] The spatial confinement of the width of the waveguide leads to lateral standing spin waves, resulting in the emergence of higher order propagating modes.^[18,19] Furthermore, both symmetric and antisymmetric spin wave mode excitations in magnonic waveguides were already shown experimentally, which can also be observed in this study at higher frequencies.^[11,12] Here, we extend the long axis of the magnonic waveguide to avoid standing spin wave patterns, and thus, we are able to show spin wave emission only from a single edge into the waveguide. Thereby, we also demonstrate STXM imaging at the higher frequencies up to 20.5 GHz. These simultaneously excited higher order modes perfectly fit the theoretical predictions as a function of static external magnetic field B_{ext} and continuous wave (CW) RF. The ultimate capabilities of time-resolved STXM with magnetic X-ray circular dichroism (XMCD) contrast provide the necessary spatial (<20 nm) and temporal (8 ps) resolution with relative phase, amplitude, and k -space information.^[20–24] The combination of time-resolved STXM and the proposed sample material and geometry permits the direct imaging of high-frequency multimode spin wave excitation and propagation above 10 GHz. The stability and reliability of the demonstrated magnonic waveguides could lay the foundation for future radar and communication systems.

Sample Design: The sample consists of a 45 μm long, 700 nm wide, and 30 nm thick waveguide of $\text{Co}_{25}\text{Fe}_{75}$ on top of the signal line of a coplanar waveguide (CPW) of copper (Cu). More details on the CoFe fabrication can be found elsewhere.^[25] **Figure 1a** shows the magnonic waveguide in red and the signal line in gray. For measurements, the right end of the waveguide is the focused area in this work. An external field B_{ext} can be applied in the x -direction up to $B_{\text{ext}} = \pm 240$ mT. Thus, spin waves are excited in the backward volume (BV) configuration; i.e., B_{ext} is parallel to the k -vector. **Figure 1b** shows the excitation scheme, where the RF current I_{RF} generates the global RF field. While B_{ext} is applied, the simulated relaxed magnetization configuration on the edge is depicted in the inset revealing local variations in the magnetization direction. The RF field can couple on these variations to excite spin waves from the edges.^[16]

Micromagnetic Simulations: Micromagnetic simulations were performed using MuMax3^[26] with the saturation magnetization $M_{\text{s}} = 1500$ KA m^{-1} , the exchange constant $A_{\text{ex}} = 13$ pJ m^{-1} , and the gyromagnetic ratio $\gamma = 176$ $\text{rad ns}^{-1} \text{T}^{-1}$ to reveal the relaxed magnetization state, as shown in **Figure 1b**.^[27]

X-Ray Microscopy with Arbitrary Waveform RF Excitation: STXM measurements were performed with polarized X-ray flashes from the BESSY II synchrotron radiation facility in a pump–probe-type experiment. These time-resolved movies were evaluated using an FFT algorithm in time and space to gain insights into the frequency domain and the corresponding k -space, respectively. Further information of the evaluation process can be found elsewhere.^[24]

Beyond previous excitation schemes,^[20] here, we developed an RF excitation that relies on AWG, effectively a fast digital-to-analog converter, as shown in **Figure 2**. To this end, the synchrotron

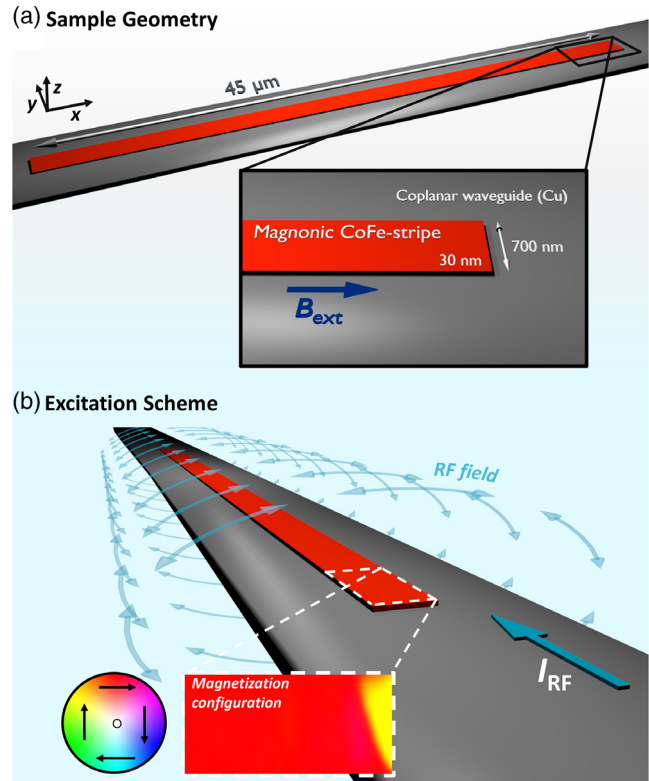


Figure 1. a) Illustration of the sample geometry. The magnonic CoFe waveguide is depicted in red and the signal line of the CPW in gray. The zoomed-in section highlights the measuring area. b) Excitation scheme for spin wave excitation. A global sinusoidal RF field is generated by the RF current I_{RF} . In addition, the initial magnetization configuration is depicted, revealing variations in the magnetization direction.

master clock f_{sync} was prescaled with an Analog Devices AD9914 direct digital synthesizer to synchronize a Keysight Technologies M8195A AWG to the pump and probe frequencies. On top of this base frame synchronization, RF excitation signals up to $f_{\text{out}} \leq 30$ GHz were generated using a custom written MATLAB software that ensures ultra-low jitter pump–probe synchronization. Subsequently, the RF signal is amplified and conducted on to the sample for spin wave excitation.

To ensure synchronization with the synchrotron source, two basic constraints need to be met. The sampling rate f_{sample} of the AWG needs to match

$$f_{\text{sample}} = \frac{P}{N} \times f_{\text{bunch}} \quad (1)$$

the synchrotron clock frequency f_{bunch} with respect to the number N of video frames to be acquired and an integer prescaling factor P . Furthermore, the RF excitation pattern needs to consist of S samples

$$S = \frac{P}{M} \quad (2)$$

with M being an integer. Any non-integer remainder in S will result in pump jitter and has to be avoided by appropriate choice

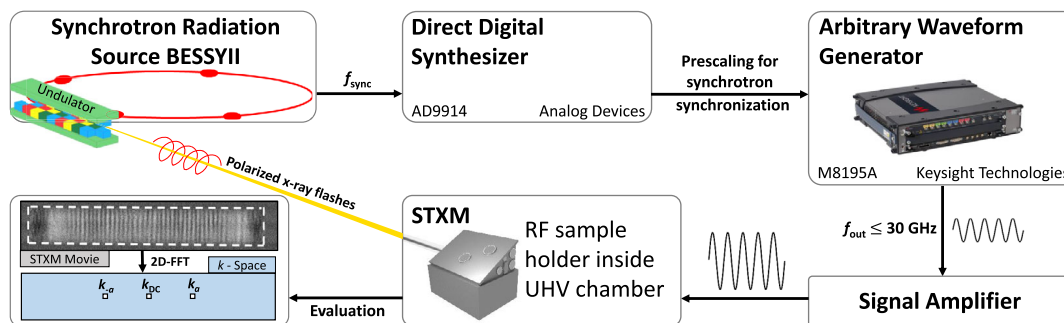


Figure 2. Schematic illustration of the signal generation and synchronization of the probing X-ray flashes and the pumping RF current. The frequency f_{sync} of the electron bunches is prescaled by a direct digital synthesizer. This signal is used as an input trigger signal for an arbitrary waveform generator, which is capable of generating signals up to $f_{\text{out}} < 30$ GHz. The amplified signal is led into the ultra-high vacuum (UHV) chamber of the STXM. Finally, an exemplary measured STXM movie is evaluated by FFT algorithms revealing frequency and k -space information.

of the other parameters. A more detailed description of the synchronization process can be found elsewhere.^[28]

First, we observe spin waves at a moderate CW frequency $f_{\text{CW}} = 12.5$ GHz, however, exceeding previous STXM capabilities.^[29] An example of such a snapshot from an STXM movie is shown in **Figure 3a** with an applied field of $B_{\text{ext}} = 4$ mT. The dashed white lines indicate the boundaries of the CoFe waveguide. The grayscale represents the magnetization component m_z . From the direct magnetization snapshot, a "zigzag"-shaped pattern already becomes visible, which hints at multiple coexisting modes. To capture relative phase and amplitude of the spin

waves in an STXM movie, we perform a pixel-wise fast Fourier transformation (FFT) and encode these quantities in color and brightness, respectively. This is shown for a field sweep between $B_{\text{ext}} = 0$ and 16 mT in **Figure 3b**. To further disentangle higher order modes and to follow their field dependency, we transform these measurements into k -space, as shown in **Figure 3c**. The three dotted arrows point out an example for $B_{\text{ext}} = 4$ mT.

From the measurements, it becomes clear that for each frequency and field set, three different modes of the waveguide are observed simultaneously. At 12.5 GHz and $B_{\text{ext}} = 4$ mT, these occur at $k_x = 0.3, 2.0,$ and $3.7 \mu\text{m}^{-1}$ where the wave

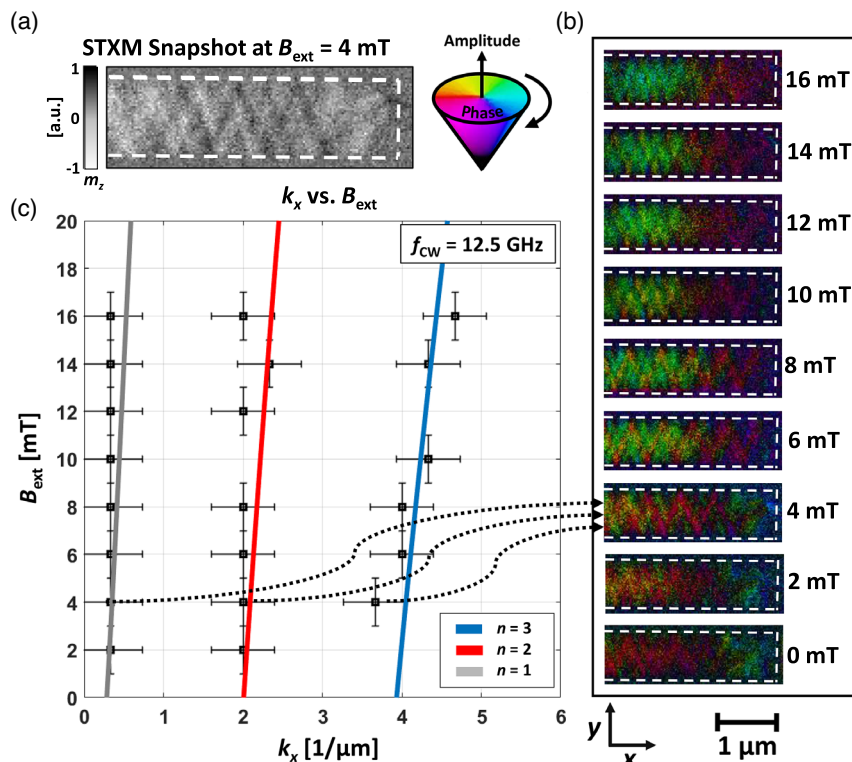


Figure 3. a) Snapshot of an STXM movie. The grayscale represents the magnetization component m_z . b) Sweep of the external field from 0 to 16 mT. Phase and amplitude maps are depicted with the shown color code. c) k -vector as a function of B_{ext} . The solid lines show the analytical theory of $n = 1, 2, 3$. Experimental data points are indicated with corresponding error bars.

vector k represents the inverse of the wavelength λ (1/m). To further understand these results, they are compared with the analytical theory of confined film structures.^[18,19,30] The physical confinement of the waveguide causes effectively pinning boundary conditions, which is considered in these calculations. Accordingly, the solid lines in Figure 3c indicate the fundamental waveguide mode $n = 1$ and the two following higher order modes $n = 2$ and 3.

The experimental data points, plotted in Figure 3c, exhibit excellent agreement with the analytical theory. The k -vector error $k_{x,\text{err}} = \pm 0.4 \mu\text{m}^{-1}$ is caused by the spatial resolution and the peak width within the k -space image. The external field was calibrated with an error of $B_{\text{err}} = \pm 1$ mT. This clearly demonstrated the reliability and the low jitter of our pump-probe excitation scheme for time-resolved STXM measurements. Furthermore, this confirms the applicability of the theory of confined magnonic waveguide structures on the nanoscale. It becomes apparent that both phase and amplitude information are crucial for interpreting spin wave propagation below $\lambda < 200$ nm correctly.

After confirming the validity of our experimental scheme and the applicability of the theoretical description, we explore the properties of our waveguide toward higher frequencies. The dispersion relation $f(k_x)$ is shown for static field of $B_{\text{ext}} = 100$ and 60 mT in Figure 4a and b, respectively. In addition, the shaded areas indicate the uncertainty due to the experimental error B_{err} in the applied magnetic bias field. Below the dispersion relation in Figure 4a, spin wave maps for two different CW frequencies $f_{\text{CW}} = 17.5$ and 20.5 GHz are shown. We find two modes for each frequency at $k_x = 0.3$ and $1.7 \mu\text{m}^{-1}$ that match the calculated dispersion relation. However, at $f_{\text{CW}} = 17.5$ GHz,

we detect $n = 1$ and 2, whereas $f_{\text{CW}} = 20.5$ GHz exhibits $n = 2$ and 3.

To exclude a limitation in maximum k , we shift the dispersion relation toward lower frequency, by reducing the magnetic bias field to $B_{\text{ext}} = 60$ mT. At this field, an excitation frequency of $f_{\text{CW}} = 15.5$ GHz was used to excite spin waves. The resulting phase and amplitude map is shown at the bottom of Figure 4b. The subsequent k -space transformation reveals four peaks at $k_x = 0.3, 1.7, 3.3,$ and $6.0 \mu\text{m}^{-1}$, which are marked in the dispersion plot. Again, we find good agreement with analytical theory and observe simultaneous existence of the mode numbers $n = 1, 2, 3,$ and 4. The largest $k_{x,n=4}$ vector corresponds to a spin wave wavelength of $\lambda_{n=4} = 170$ nm.

This shows that the STXM does not suffer from the same k -space limitations as measurement techniques that rely on visible light, and is indeed capable of detecting spin waves, also beyond the frequencies of 10 GHz.^[31] This is especially true for nanoscale sample geometries where confinement effects lead to a more complex dispersion behavior, as shown in our measurements. Even the shown capabilities of multimode transport and, thus, higher data rates in such magnonic waveguides become increasingly important in the area of, for example, communication and radar systems where data throughput and precise positioning are crucial for future competitive applications.

In conclusion, we have demonstrated the direct imaging of magnons in magnonic CoFe waveguides up to 20.5 GHz. A straight forward process for generating RF signals and synchronizing X-ray flashes with RF currents using arbitrary waveform generation (AWG) has been described schematically. In addition, a field-dependent analytical theory was confirmed experimentally

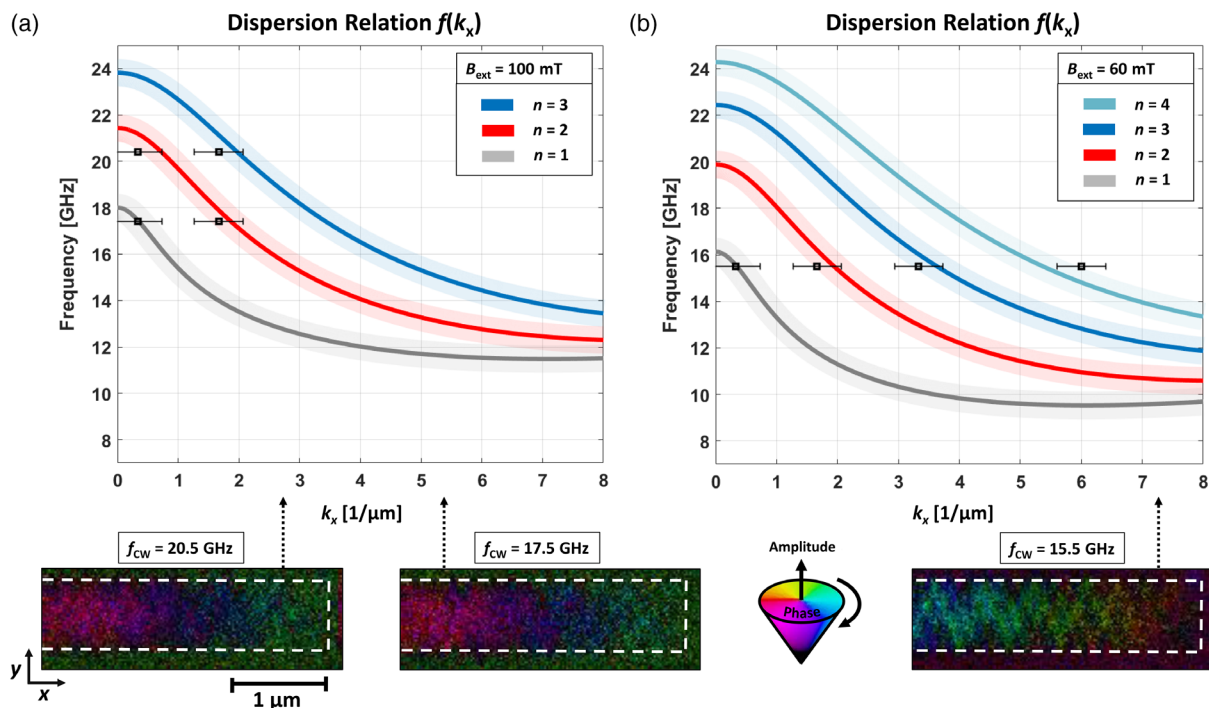


Figure 4. a) Dispersion relation $f(k_x)$ for $B_{\text{ext}} = 100$ mT with experimental results for $f_{\text{CW}} = 17.5$ and 20.5 GHz. The faded lines represent the error of the external field for the corresponding mode numbers. Phase and amplitude maps are shown at the bottom. b) Dispersion relation $f(k_x)$ for $B_{\text{ext}} = 60$ mT with experimental results for $f_{\text{CW}} = 15.5$ GHz. The phase and amplitude map is shown at the bottom.

by an external field sweep between $B_{\text{ext}} = 0 - 16$ mT at $f_{\text{CW}} = 12.5$ GHz. In doing so, the waveguide mode number $n = 1$ and the following higher order modes $n = 2$ and 3 were observed, fitting the theoretical predictions. Furthermore, the analytic dispersion relation for static external fields of $B_{\text{ext}} = 60$ and 100 mT was validated at the excitation frequencies $f_{\text{CW}} = 15.5, 17.5$ and 20.5 GHz. Finally, this work is not only a verification of good agreement between theory and experiment, but also a demonstration of the capabilities of time-resolved STXM. By presenting high-frequency magnonics, this approach opens the door for new possibilities regarding direct imaging of high-frequency magnetization dynamics in nanoscaled magnonic devices or fundamental quantum phenomena in the field of magnetic wave physics.

Acknowledgements

The authors would like to thank Michael Bechtel for support during beam times and Helmholtz-Zentrum Berlin for the allocation of synchrotron radiation beam time. N.T., M.W., and J.G. acknowledge financial support by the Federal Ministry of Education and Research of Germany in the framework of DynaMAX (project number 05K18EYA). Open access funding enabled and organized by Projekt DEAL.

Conflict of Interest

The authors declare no conflict of interest.

Keywords

magnetism, magnonics, nanoscale, spin waves, X-ray microscopy

Received: July 30, 2020

Revised: August 26, 2020

Published online: September 4, 2020

- [1] S. Neusser, D. Grundler, *Adv. Mater.* **2009**, 21, 2927.
- [2] A. V. Chumak, A. A. Serga, B. Hillebrands, *J. Phys. D: Appl. Phys.* **2017**, 50, 244001.
- [3] A. V. Chumak, V. I. Vasyuchka, A. A. Serga, B. Hillebrands, *Nat. Phys.* **2015**, 11, 453.
- [4] A. V. Chumak, A. A. Serga, B. Hillebrands, *Nat. Commun.* **2014**, 5, 4700.
- [5] B. Lenk, H. Ulrichs, F. Garbs, M. Münzenberg, *Phys. Rep.* **2011**, 507, 107.
- [6] C. Sturm, W. Wiesbeck, *Proc. IEEE* **2011**, 99, 1236.
- [7] T. Mitomo, N. Ono, H. Hoshino, Y. Yoshihara, *IEEE J. Solid-State Circuits* **2010**, 45, 928.
- [8] A. Meta, P. Hoogeboom, L. P. Ligthart, *IEEE Trans. Geosci. Remote Sens.* **2007**, 45, 3519.
- [9] C. R. Berger, B. Demissie, J. Heckenbach, P. Willett, S. Zhou, *IEEE J. Sel. Top. Signal Process.* **2010**, 4, 226.
- [10] E. Bankowski, T. Meitzler, R. S. Khymyn, V. S. Tiberkevich, A. N. Slavin, H. X. Tang, *Appl. Phys. Lett.* **2015**, 107, 122409.
- [11] N. Träger, P. Gruszecki, F. Lisiecki, F. Groß, J. Förster, M. Weigand, H. Glowinski, P. Kuswik, J. Dubowik, M. Krawczyk, J. Gräfe, *Nanoscale* **2020**, 12, 17238.
- [12] O. Büttner, M. Bauer, C. Mathieu, S. O. Demokritov, B. Hillebrands, P. A. Kolodin, M. P. Kostylev, S. Sure, H. Dötsch, V. Grimalsky, Y. Rapoport, A. N. Slavin, *IEEE Trans. Magn.* **1998**, 34, 1381.
- [13] V. E. Demidov, S. O. Demokritov, K. Rott, P. Krzyszczo, G. Reiss, *Phys. Rev. B* **2008**, 77, 064406.
- [14] P. Clausen, K. Vogt, H. Schultheiss, S. Schäfer, B. Obry, *Appl. Phys. Lett.* **2011**, 99, 162505.
- [15] W. S. Ishak, E. Reese, E. Huijter, *Circuits Syst. Signal Process.* **1985**, 4, 285.
- [16] F. B. Mushenok, R. Dost, C. S. Davies, D. A. Allwood, B. J. Inkson, G. Hrkac, V. V. Kruglyak, *Appl. Phys. Lett.* **2017**, 111, 042404.
- [17] V. V. Kruglyak, P. S. Keatley, A. Neudert, M. Delchini, R. J. Hicken, J. R. Childress, J. A. Katine, *Phys. Rev. B* **2008**, 77, 172407.
- [18] K. Y. Guslienko, S. O. Demokritov, B. Hillebrands, A. N. Slavin, *Phys. Rev. B* **2002**, 66, 132402.
- [19] T. Brächer, P. Pirro, B. Hillebrands, *Phys. Rep.* **2017**, 699, 1.
- [20] M. Weigand, *Realization of a New Magnetic Scanning X-ray Microscope and Investigation of Landau Structures Under Pulsed Field Excitation*, Cuvillier Verlag, Göttingen, Germany **2015**.
- [21] J. Gräfe, M. Weigand, N. Träger, G. Schütz, E. J. Goering, M. Skripnik, U. Nowak, F. Haering, P. Ziemann, U. Wiedwald, *Phys. Rev. B* **2016**, 93, 104421.
- [22] K. Litzius, I. Lemesh, B. Krüger, P. Bassirian, L. Caretta, K. Richter, F. Büttner, K. Sato, O. A. Tretiakov, J. Förster, R. M. Reeve, *Nat. Phys.* **2016**, 13, 170.
- [23] S. Woo, K. Litzius, B. Krüger, M.-Y. Im, L. Caretta, K. Richter, M. Mann, A. Krone, R. M. Reeve, M. Weigand, *Nat. Mater.* **2016**, 15, 501.
- [24] F. Groß, N. Träger, J. Förster, M. Weigand, G. Schütz, J. Gräfe, *Appl. Phys. Lett.* **2019**, 114, 012406.
- [25] H. Glowinski, F. Lisiecki, P. Kuşwik, J. Dubowik, F. Stobiecki, *J. Alloys Compd.* **2019**, 785, 891.
- [26] A. Vansteenkiste, J. Leliaert, M. Dvornik, M. Helsen, F. Garcia-Sanchez, B. V. Waeyenberge, *AIP Adv.* **2014**, 4, 107133.
- [27] M. A. W. Schoen, J. Lucassen, H. T. Nembach, T. J. Silva, B. Koopmans, C. H. Back, J. M. Shaw, *Phys. Rev. B* **2017**, 95, 134410.
- [28] J. Gräfe, M. Weigand, B. Van Waeyenberge, A. Gangwar, F. Groß, F. Lisiecki, J. Rychly, H. Stoll, N. Träger, J. Förster, F. Stobiecki, J. Dubowik, H. Klos, M. Krawczyk, C. H. Back, E. J. Goering, G. Schütz, *Proc. SPIE* **2019**, 11090, 1109025.
- [29] S. Bonetti, R. Kukreja, Z. Chen, D. Spoddig, K. Ollefs, C. Schöppner, R. Meckenstock, A. Ney, J. Pinto, R. Houanche, J. Frisch, J. Stöhr, H. A. Dürr, H. Ohldag, *Rev. Sci. Instrum.* **2015**, 86, 093703.
- [30] B. A. Kalinikos, A. N. Slavin, *J. Phys. C: Solid State Phys.* **1986**, 19, 7013.
- [31] G. Dieterle, J. Förster, H. Stoll, A. S. Semisalova, S. Finizio, A. Gangwar, M. Weigand, M. Noske, M. Fähnle, I. Bykova, J. Gräfe, D. A. Bozhko, H. Y. Musiienko-Shmarova, V. Tiberkevich, A. N. Slavin, C. H. Back, J. Raabe, G. Schütz, S. Wintz, *Phys. Rev. Lett.* **2019**, 122, 117202.